



SOFTWARE REPORT

Ot2Rec: A Semi-Automatic, Extensible, Multi-Software Tomographic Reconstruction Workflow

Neville B.-y. Yee¹ , Elaine M. L. Ho¹ , Win Tun^{2,3} , Jake L. R. Smith^{4,5} , Maud Dumoux⁴ , Michael Grange^{4,5} , Michele C. Darrow^{1,6} and Mark Basham^{1,3}

¹Artificial Intelligence & Informatics, Rosalind Franklin Institute, Harwell Campus, Didcot, OX11 0FA, UK

²Faculty of Medical Sciences, Newcastle University, Newcastle upon Tyne, NE1 7RU, UK

³Diamond Light Source Ltd., Diamond House, Harwell Campus, Didcot, OX11 0DE, UK

⁴Structural Biology, Rosalind Franklin Institute, Harwell Campus, Didcot, OX11 0FA, UK

⁵Division of Structural Biology, Wellcome Centre for Human Genetics, University of Oxford, Oxford, OX3 7BN, UK

⁶SPT Labtech, Melbourn Science Park, Cambridge Road, Melbourn, SG8 6HB, UK

Received xx xxx xxxx

Keywords: cryo-electron tomography, image processing, cryo-electron microscopy

Abstract

Electron cryo-tomography (cryo-ET) is an imaging technique for probing 3D structures with at the nanometre scale. This technique has been used extensively in the biomedical field to study the complex structures of proteins and other macromolecules. With the advancement in technology, microscopes are currently capable of producing images amounting to terabytes of data per day, posing great challenges for scientists as the speed of processing of the images cannot keep up with the ever-higher throughput of the microscopes. Therefore, automation is an essential and natural pathway on which image processing – from individual micrographs to full tomograms – is developing. In this paper, we present Ot2Rec, an open-source pipelining tool which aims to enable scientists to build their own processing workflows in a flexible and automatic manner. The basic building blocks of Ot2Rec are plugins which follow a unified API structure, making it simple for scientists to contribute to Ot2Rec by adding features which are not already available. In this paper, we also present three case studies of image processing using Ot2Rec, through which we demonstrate the speedup of using a semi-automatic workflow over a manual one, the possibility of writing and using custom (prototype) plugins, and the flexibility of Ot2Rec which enables the mix-and-match of plugins. We also demonstrate, in the supplementary information, a built-in reporting feature in Ot2Rec which aggregates the metadata from all process being run, and output them in the Jupyter Notebook and/or HTML formats for quick review of image processing quality. Ot2Rec can be found at <https://github.com/rosalindfranklininstitute/ot2rec>.

Impact Statement

The field of cryo electron tomography has grown substantially in recent years, bringing about new advances in hardware and software which enable visualisation of cell and tissue architecture and proteins found in their native context. These same advances have, in some ways, stratified the field into those with access and those without. On the software side, this has emphasised the need for open-source options that do not require high levels of computational literacy to access. Additionally, it has highlighted the need for ways to both mix-and-match software for easy prototyping and comparisons between parameters and methods. Ot2Rec addresses these needs through a simple, unified plugin structure allowing the addition of existing software or the development of new and does so in a way which democratises access.

¹ © The Author(s) 2021. Published by Cambridge University Press. This is an Open Access article, distributed under the terms of the Creative Commons Attribution licence (<http://creativecommons.org/licenses/by/4.0/>), which permits unrestricted re-use, distribution, and reproduction in any medium, provided the original work is properly cited.

2 1. Introduction

3 1.1. Cryo-ET & data acquisition

4 Electron cryo-tomography (cryo-ET), is an imaging technique that produces three-dimensional outputs
 5 in the nanometre resolution range^(1,2). In the biomedical field, it has been used to study heterogeneous
 6 purified proteins using sub-tomogram averaging^(3,4), structures within thin or smaller cells⁽⁵⁾, the edges
 7 of larger cells⁽⁶⁾, and more recently in conjunction with cryo focused ion beam milling (cryoFIB),
 8 sub-cellular structures and proteins⁽⁷⁻⁹⁾.

9 The sample must first be vitrified using either traditional plunge freezing methods⁽¹⁰⁾ or high
 10 pressure freezing for larger samples⁽¹¹⁾. In some cases, the frozen sample is subsequently thinned by
 11 cryosectioning⁽¹²⁾ or cryoFIB milling⁽¹³⁻¹⁵⁾. These cryogenic specimen preparation techniques alleviate
 12 the need for chemical fixatives and stains which are commonly used to preserve biological structures
 13 and bolster contrast in room temperature volume electron microscopy (vEM) techniques^(16,17).

14 During data collection images are taken at a series of angles by tilting the specimen, typically in the
 15 range of approximately -60° to $+60^\circ$ with a 2° to 5° step between tilts, though many tilt acquisition
 16 schemes exist to ration exposure of the specimen⁽¹⁸⁾. In all cases, a portion of information is not col-
 17 lected due to mechanical constraints of the microscope stage and increasing specimen thickness during
 18 tilting. This leads to a missing wedge or cone of information in Fourier space and an elongation of the
 19 resultant reconstructed data in the direction of the electron beam in real space⁽¹⁹⁾.

20 1.2. Current image processing workflow for cryo-ET

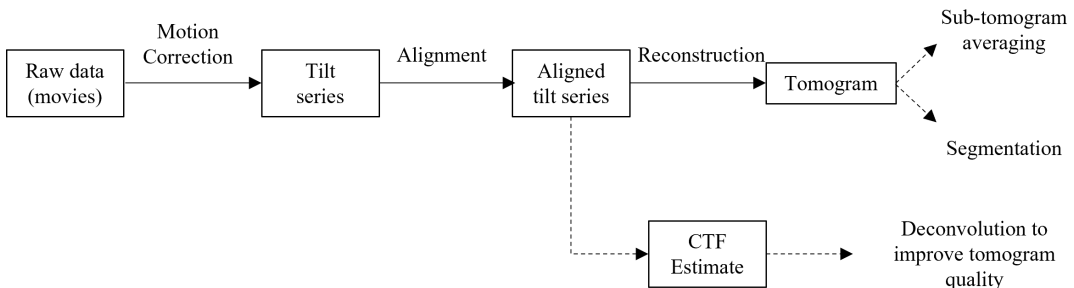


Figure 1. Typical image processing tasks for reconstructing tomograms from raw micrograph movies.
 Key: boxes - datasets, solid arrows - processes necessary for tomogram reconstruction, dotted arrows
 - optional processes.

21 Several stages of image processing tasks are required to produce tomograms from raw micrograph
 22 movies (Figure 1). Many software tools exist for each stage, which have been reviewed recently by Pyle
 23 and Zanetti⁽²⁰⁾. Raw micrograph movies at each tilt angle are first motion-corrected to compensate for
 24 specimen movement during acquisition. Individual frames of the movies recorded at each angle are
 25 aligned and averaged to produce a single image for each tilt angle. These motion-corrected images
 26 are sorted in order of their tilt angles to produce a tilt series. Tilt series projections are then aligned
 27 to ensure the rotation axis is consistent between projections. This can be performed with or without
 28 fiducial markers. At this stage, the contrast transfer function (CTF) can be optionally estimated from
 29 the aligned tilt series, and deconvolved with the tomogram at later stages to improve the image quality.
 30 Aligned projections are then reconstructed into tomograms, which provide the 3D representation of the
 31 specimen. Post-processing strategies can then be applied to the tomograms, which will be dependent

Software/Feature	TomoBear	TomoRobot	EMAN2	Scipion3	Warp	Ot2Rec
Open-source?	Yes	Yes	Yes	Yes	Yes	Yes
Programming language	Matlab	Python, Matlab	Python	Python	C#, C++, CUDA C	Python
File formats	EER, MRC, Tiff	MRC, Tiff	EER, MRC, Tiff, proprietary file formats	raw, MRC, Tiff, jpeg, proprietary formats	MRC, Tiff, EM	EER, MRC, Tiff
GUI	No	No	Yes	Yes	Yes	Yes
Motion Correction	MotionCor2	MotionCor2	EMAN2	MotionCor2, Xmippromo, FlexAlign.	Warp	MotionCor2
Alignment	Dynamo, IMOD	modified Dynamo	EMAN2	IMOD	Warp	AreTomo, IMOD
Reconstruction	IMOD	Relion	EMAN2	IMOD, Tomo3D, AreTomo, Nova-CTF	Warp	AreTomo, IMOD, Savu
CTF estimation	Gctf	CTFFind4	EMAN2	Cistem, CTFFIND4, Gctf, IMOD, Emantom	Warp	CTFFind4, CTFSim
Dataset requirements	Unspecified	Fiducials required Dose-symmetric tilt-scheme starting at 0	Unspecified	Unspecified	Unspecified	Unspecified
References	(21)	(22)	(23)	(24)	(25)	this work

Table 1. Comparison of cryo-ET reconstruction pipelines.

32 on the specific research question. This often involves sub-tomogram averaging (STA) to obtain high-
 33 resolution structures of repeating structures in the tomogram, or segmentation to determine spatial
 34 relationships between structures.

35 *1.3. Existing cryo-ET pipelines*

36 The image processing tasks required to reconstruct tomograms from the movies are generally consistent
 37 for different experiments, though the post-processing stages afterwards often require more customisation.
 38 However, many software tools exist for each stage of the reconstruction process, each with their
 39 own disparate data structures, standards, and user interfaces. Users must learn how to use each indi-
 40 vidual tool and adapt their data structures to fit the specific software package, increasing the barrier to
 41 trying alternative tools which may have better performance or functionality. Therefore, pipelines which
 42 manage the data flow and provide a unified interface for several software tools would enable easier
 43 combination and trialling of the different software tools to optimise reconstruction outcomes.

44 A few pipelines already exist to automate the reconstruction process within a single framework,
 45 to varying degrees of customisation (Table 1). Generally, these pipelines were developed to automate
 46 reconstruction for datasets collected within a single research group, and thus, do not enable substi-
 47 tution of different tools developed elsewhere. These pipelines include TomoBear⁽²¹⁾, TomoRobot⁽²²⁾,
 48 EMAN2⁽²³⁾, and Warp⁽²⁵⁾. Scipion 3.0 gives users a wide range of software tools to choose in their
 49 framework and offers a user-friendly workflow builder in their graphical user interface (GUI). How-
 50 ever, accessing the Scipion tools programmatically is not straightforward, so automation of the process
 51 is more challenging.

52 *1.4. Motivation*

53 Here, we present Ot2Rec, a pipeline for reconstruction of cryo-ET tilt series which allows users to
 54 combine different software tools within a single framework. Ot2Rec can be used via a GUI but can also
 55 be automated programmatically if required. Ot2Rec is easily extensible through its plugin architecture,
 56 and published open-source under the Apache v2.0 license. Ot2Rec is developed as an open-source
 57 project with a strong focus on user involvement. We welcome contributions from users and developers
 58 alike, our contributors guide is available on our [Github Wiki](#). A written tutorial guiding users through
 59 reproducing one of our case studies is available in the Supplementary Information, in addition to a
 60 guide to writing Ot2Rec plugins for developers. These documents are also online on our wiki at <https://github.com/rosalindfranklininstitute/ot2rec/wiki>.

62 2. Development philosophy & features

63 Ot2Rec was developed to achieve three key characteristics of a tomography reconstruction pipeline,
 64 with the ultimate aim of fully automating tomography reconstruction to obtain high quality tomograms.
 65 Firstly, the pipeline had to offer different routes to combine tools for each stage of tomogram recon-
 66 struction. The pipeline had to be user-friendly and accessible to users without programming experience.
 67 Finally, a mechanism to evaluate all tilt series at a glance was also required. These functions together
 68 provide the framework for which a completely automated tomogram reconstruction pipeline can be
 69 built, where the optimum combination of software tools and parameters can be automatically selected
 70 and applied to several tilt series at once, with minimal user intervention. The following sections describe
 71 the design choices that were made towards achieving this functionality in Ot2Rec.

72 2.1. Different routes to tomogram reconstruction

73 2.1.1. Plugin architecture

74 In Ot2Rec, the basic program infrastructure is designed such that each feature is a standalone plugin,
 75 which has minimal interaction with other plugins. Such design is beneficial for developers as a fault in
 76 one plugin does not directly cause other plugins to fail, making further development and maintenance
 77 easier. This plugin architecture also facilitates extension of Ot2Rec to cover other image processing
 78 tools, whilst maintaining easy integration with existing workflows.

79 Each plugin performs one task within the reconstruction process, e.g., motion correction or align-
 80 ment. The plugin has two main subroutines, one to capture user input and configure the parameters for
 81 the task to be performed, and the other which generates the commands to run the task on all tilt series.
 82 Each plugin follows a simple yet unified structure for its application programming interface (API): a
 83 Python class which encapsulates all the essential plugin-specific methods, followed by subroutines that
 84 enable the plugin to communicate with the Ot2Rec main API. These subroutines are called and exe-
 85 cuted directly as entry-points by users. This well-defined, simple structure is helpful for developers and
 86 users alike as they become accustomed to the patterns of using Ot2Rec.

87 Plugins were chosen based on the software tools already used by users in our institute. The nine
 88 plugins currently available in Ot2Rec 0.2 are:

- 90 • Motion Correction
 - 91 – MotionCor2⁽²⁶⁾
- 92 • CTF Estimation and Deconvolution
 - 93 – CTFFind4^(27,28)
 - 94 – CTFSim (based on⁽²⁸⁾; described in Section 5.2)
 - 95 – RLDeconv (described in Section 5.2)
- 96 • Tilt series alignment
 - 97 – IMOD^(29,30)
 - 98 – AreTomo⁽³¹⁾
- 99 • Reconstruction
 - 100 – IMOD^(29,30)
 - 101 – AreTomo⁽³¹⁾
 - 102 – Savu⁽³²⁾

103 2.1.2. Metadata handling

104 Metadata are small files used to record the locations and other useful information about actual data
 105 being processed. Metadata often plays a key role in a multi-step computational workflow as it defines
 106 how the data are linked to each other. Metadata generated from various software and processes are
 107 often incompatible (for instance, having different headers or different metadata file formats) creating
 108 obstructions in data flow. This is a currently known problem in the electron tomography community

109 – there are many workflows and packages which use different and incompatible metadata formats,
 110 making interoperability between separate software packages extremely challenging.

111 In view of this, Ot2Rec has been designed with a central philosophy of unified metadata structure.
 112 To use Ot2Rec for image processing, the user first runs the command `o2r.new` with which Ot2Rec
 113 aggregates the master metadata that includes the path to the raw images (micrographs) and the tilt series
 114 indices of the individual micrographs.

115 In subsequent processing steps (i.e. plugins), Ot2Rec stores the metadata files from the individual
 116 programs and outputs an independent metadata file. This metadata file is a human-readable easily parsed
 117 YAML format that carries essential information for the next steps.

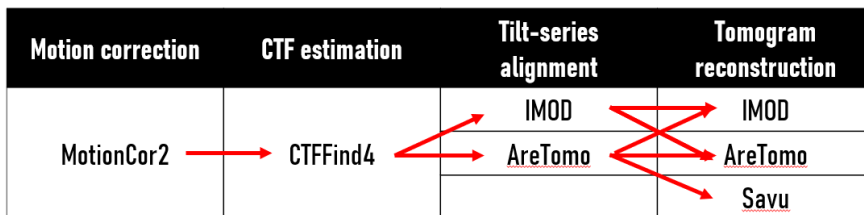


Figure 2. Standard workflows implemented in Ot2Rec. Red arrows denote possible branches of the workflow, which currently covers all permutations of existing implemented plugins (though not necessarily all available options within a software e.g., IMOD).

118 The unified internal metadata system allows workflows to be built flexibly by interchanging the
 119 different plugins for each task. Whilst several default workflows are implemented in the package (cf.
 120 Fig. 2), for instance, MotionCor2 → IMOD (alignment + reconstruction), or MotionCor2 → IMOD
 121 (alignment) → Savu (reconstruction), the "network" of possible routes can continue to grow as more
 122 plugins are implemented into Ot2Rec. This flexibility and customisation allows the user to maximise
 123 both result quality and computational performance.

124 As image processing programs each have different parameters, the quality of the output and com-
 125 putational performance can vary vastly depending on the chosen parameters. With a flexible workflow,
 126 users can choose the tools that best suit their purposes and test different parameters provided by the
 127 same tool. They can also compare the results using the reporting feature of Ot2Rec. Once the user has
 128 completed a comparative study, preferably using a small, representative subset of their data, they can
 129 continue to process the rest of their data using the optimal workflow and parameters they have identified.

130 2.2. User-friendliness

131 Graphical user interfaces (GUI) are a means for a program to communicate with the user. Its usage can
 132 range from the collection of essential parameters to the interactive display of results.

133 In Ot2Rec, a Linux-based program, since the building blocks are the individual plugins which have
 134 a wide range of parameters as inputs, a GUI is necessary to remove the use of command-line flags.
 135 For this reason, we have implemented MagicGUI⁽³³⁾ as Ot2Rec's GUI for gathering parameters from
 136 users. One of the biggest benefits of using a simple GUI over the command-line is that parameters can
 137 be presented in a more human-readable and descriptive way rather than using internal variable names,
 138 which in many cases need to be brief. Another benefit of using a GUI as the first point of communication
 139 between the user and the program is that since the parameters are more descriptively presented, the
 140 chance of incorrect inputs can be reduced, as additional information can be displayed alongside the
 141 parameter inputs for explanation.

142 **2.3. Report generation**

143 Comparison of the outputs of different tomogram reconstruction workflows is facilitated in Ot2Rec by
 144 automatically generated reports, which contain a workflow diagram describing the plugins that have
 145 been applied, selected input parameters, and performance metrics for each plugin. This report is gener-
 146 ated for the entire project, allowing the user to evaluate the reconstruction process for all tilt series in
 147 the project at a glance. These reports can be generated in a document, slideshow or Jupyter notebook
 148 format⁽³⁴⁾, allowing users to customise how they would like to interact with the report. Reports for all
 149 the case studies in this work are included in the Supplementary Information as examples.

150 **3. Case Studies**

151 **3.1. Case Study 1: Semi-automatic processing of large datasets**

152 Tomographic image processing is often performed manually, with users processing one tilt-series at
 153 a time. Scripts can be written to automate some of the procedures especially for those being carried
 154 out using command-line programs, such as MotionCor2, though this can be difficult and frustrating
 155 for many users without a programming background. Ot2Rec enables users to automatically set up and
 156 apply a reconstruction workflow to entire datasets of several tilt series at once, without any scripting
 157 or individual processing of datasets. A report can be automatically generated at the end for the user to
 158 evaluate the performance of the reconstruction process on all tilt series at a glance.

159 Here, we demonstrate the use of Ot2Rec to reconstruct tomograms from the EMPIAR-10364
 160 dataset⁽³⁵⁾. This dataset consisted of 17 tilt series of *E. coli* minicells acquired on a Titan Krios at the
 161 electron Bio-Imaging Centre, Diamond Light Source. Each tilt series had 60 projections from -60° to
 162 $+60^\circ$ in 2° increments. The movie taken at each tilt angle contained 5 frames. Images were binned by
 163 a factor of 2 at the alignment step for faster processing, and no binning was applied in reconstruction
 164 for a final bin factor of 2x between the raw data and tomogram. Motion correction was performed with
 165 MotionCor2, and alignment and weighted back-projection (WBP) reconstruction were performed with
 166 IMOD. See Section 5 for more details.

167 Ot2Rec substantially reduced the amount of user intervention required to process tomograms as con-
 168 figured workflows are automatically applied to all tilt series in the dataset. Typically, the user would
 169 have to take each individual tilt series through several software packages, which is feasible for exper-
 170 iments with a few tilt series, but quickly becomes a bottleneck when scaling to dozens or hundreds
 171 of tilt series. This case study shows that typical reconstruction workflows with popular software tools
 172 can be deployed with Ot2Rec for large datasets, with the potential for automated parameter tuning to
 173 determine the optimum reconstruction workflow in the future.

174 The report generated summarised the performance of each step in the reconstruction process. First,
 175 a diagram showing the processes run on the dataset is shown (Figure 3a). The shifts between frames
 176 reported by MotionCor2 were within 1–2 pixels and fairly uniform across all tilt series (Figure 3b).
 177 The average shifts between patches from the alignment patch-tracking step were between 10 and 38
 178 Angstroms, and all tilt series had relatively similar shifts (Figure 3c). The report also contains represen-
 179 tative thumbnails of the central x-y, x-z, and y-z slices of every tomogram, allowing users to visually
 180 assess all tomograms at once. The full report for this case study is available in the Supplementary
 181 Information.

182 **3.2. Case Study 2: Demonstration and testing of prototype features**

183 Implementing custom plugins in Ot2Rec enables rapid development and deployment of bespoke algo-
 184 rithms and tools which can easily be integrated into existing tomogram reconstruction workflows. This
 185 case study demonstrates the results of a custom plugin called CTFSim, and how this bespoke tool was
 186 used in conjunction with other existing Ot2Rec plugins to enhance the quality of the reconstructed
 187 tomograms.

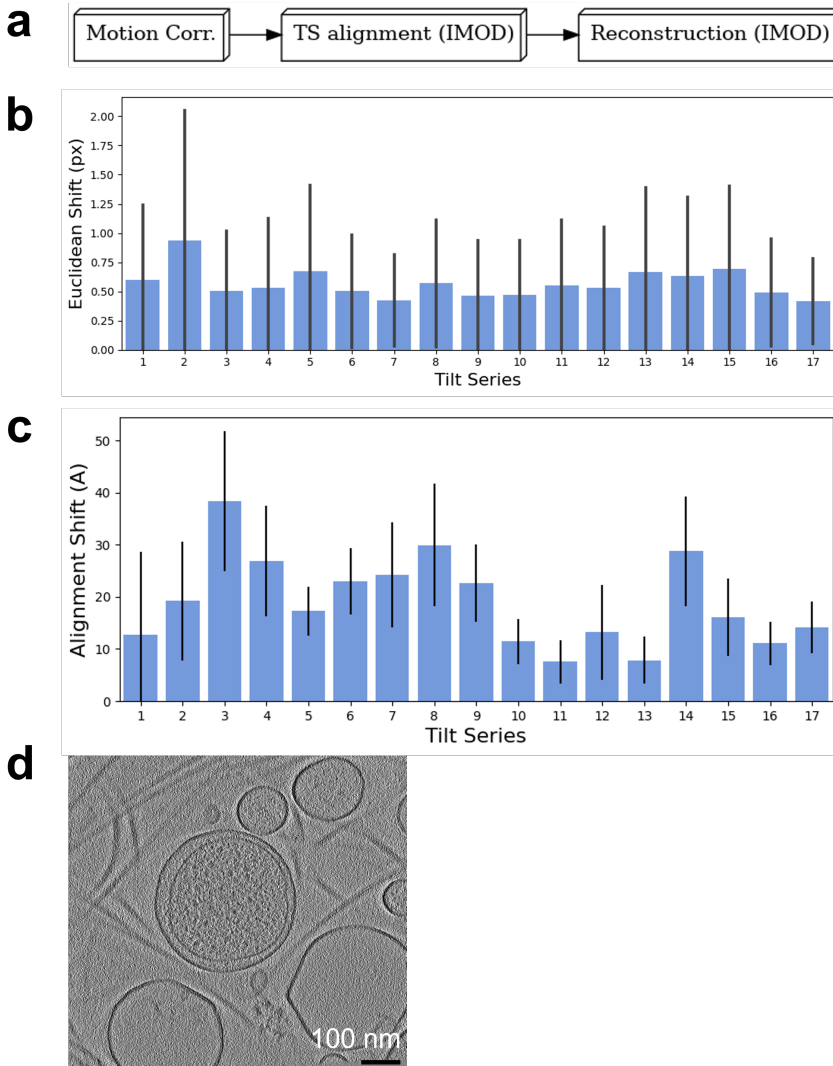


Figure 3. All tilt series in EMPIAR-10364 could be reconstructed at once in *Ot2Rec* and evaluated at a glance with the automatically generated report, some sections of which are highlighted below. (a) Workflow diagram for processes performed in Case Study 1. (b) Means and standard deviations of motion correction shifts between movie frames for all tilt series. (c) Means and standard deviations of alignment shifts between patches (L_2 -norm) for all tilt series. (d) Central x-y slice of tomogram from tilt series 18 in EMPIAR-10364, with a Gaussian blur filter applied ($\sigma = 2.0$ px $\approx 8.972\text{\AA}$). The full report is included in the Supplementary Information.

188 This case study investigated the use of deconvolution to improve contrast with the CTF estimated
 189 from CTFSim on tomograms of human choriocarcinoma cells (Figure 4). Images were acquired on a
 190 Titan Krios at the electron Bio-Imaging Centre, Diamond Light Source. Each tilt series had 41 pro-
 191 jections taken at -53° to $+27^\circ$ degrees in increments of 2° . *Ot2Rec* was used for motion correction,
 192 alignment, and reconstruction of the tomograms for all tilt series in the dataset. The tomograms were
 193 then deconvolved using the CTF estimated with the custom *Ot2Rec* plugin CTFSim (based on^(28,47);
 194 see Methods for details).

195 The improvement in image quality was measured using the contrast-to-noise ratio (CNR)⁽³⁶⁾. Briefly,
 196 the signal was segmented from the background by thresholding the grey values with the automatically
 197 determined Otsu's threshold⁽³⁷⁾. The grey value distributions in the segmented signal and background
 198 regions were used to calculate the CNR.

199 The deconvolved tomograms showed improved contrast compared to the original, as shown visually
 200 and as measured by improved contrast-to-noise ratios (CNR) in the deconvolved images (Figure 4).
 201 CNR was higher in the deconvolved tilt series compared to non-deconvolved, with the largest increase
 202 in CNR seen in tilt series 12 with deconvolution increasing CNR by 65.6% over the original tomogram.

203 3.3. Case Study 3: Optimisation of tomogram reconstruction workflow

204 Reconstruction of tomograms is a multi-stage process, where the final tomogram quality is affected by
 205 the results of earlier stages. Therefore, optimisation of the entire workflow at each stage is necessary
 206 to obtain the best results. Ot2Rec provides the framework for this optimisation by enabling users to
 207 mix-and-match different software tools on the same tilt series, and compare these results in a single
 208 report.

209 In this case study, different combinations of alignment and reconstruction tools were applied to the
 210 same dataset, and Ot2Rec reports were generated to compare the performance of each (Figure 5). This
 211 case study consisted of 23 tilt series composed of 41 projection images each ranging from -60° to $+60^{\circ}$
 212 degrees.

213 After motion-correction, fiducial-less alignment of the tilt series was performed with either IMOD
 214 or AreTomo, followed by reconstruction with either IMOD simultaneous iterative reconstruction tech-
 215 nique (SIRT), AreTomo simultaneous algebraic reconstruction technique (SART), or Savu conjugate
 216 gradient least squares (CGLS) reconstruction. Different combinations of alignment and reconstruction
 217 methods were expected to produce different results, which will be investigated in this section. The full
 218 reports for this case study are available in the Supplementary Information.

219 The shifts reported at the motion correction stage were found to be much larger for tilt series 13
 220 onwards (Figure 6a), indicating a potential issue with tilt series acquisition from this and future datasets
 221 in the experiment. Shifts between patches in alignment were also larger overall for tilt series 13 onwards
 222 compared to the earlier datasets (Figure 6b). Inspection of the tilt series data showed obstructed views at
 223 high tilt angles for those affected by large motion correction shifts. In the future, Ot2Rec could include
 224 metrics to determine low quality tilt angles to be excluded.

225 An example tomogram (tilt series 18) affected by the large shifts observed in motion correction was
 226 chosen to demonstrate differences in outcomes associated with each workflow (Figure 5b). Savu CGLS
 227 reconstruction failed with the IMOD aligned data, but not with the AreTomo alignment, and the resul-
 228 tant tomogram had reasonable image quality. However, the CGLS reconstruction had lower contrast
 229 than the SIRT or SART reconstruction methods of IMOD or AreTomo. Reconstruction with AreTomo's
 230 SART was successful for both alignment methods (IMOD and AreTomo) with very few visual differ-
 231 ences observed between the two outcomes. The IMOD SIRT reconstruction using IMOD alignments
 232 also produces a reasonable output which is visually similar to the AreTomo SART reconstructions cre-
 233 ated from either IMOD or AreTomo alignments. IMOD reconstruction using AreTomo alignments are
 234 not currently supported in Ot2Rec, but will be in the future.

235 4. Discussion

236 Ot2Rec enables reconstruction of tomograms from raw micrograph movies using a range of software
 237 tools, all within a single framework. This pipeline is distinct from available alternatives as users can
 238 choose different combinations of software tools to suit their specific experiment and automatically
 239 apply their workflow to several tilt series at once. Metadata is recorded at each stage and is easily

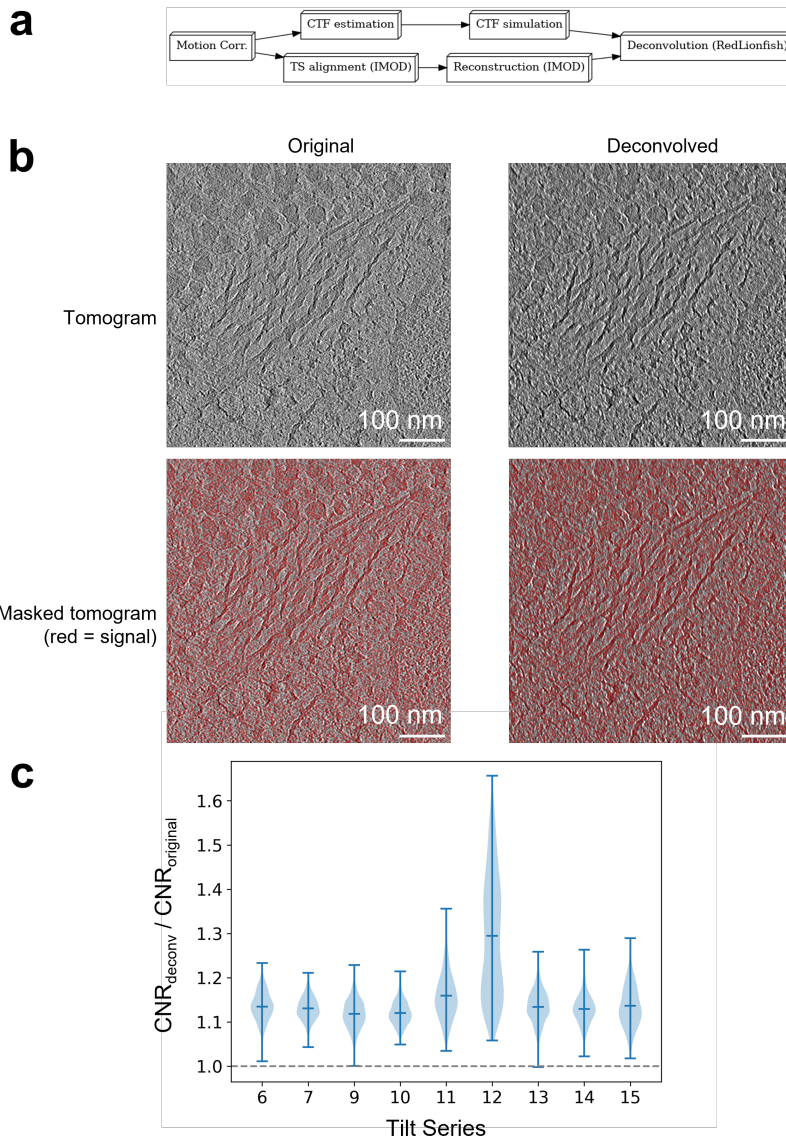


Figure 4. PSF simulation and deconvolution implemented as custom plugins in *Ot2Rec* can be easily integrated into existing image processing workflows. Deconvolution improved image quality of all tomograms in this case study of human choriocarcinoma cells. (a) Workflow diagram for processes performed in Case Study 2. (b) Thumbnails showing an example original and deconvolved tomogram (tilt series 9), unmasked (top row) and masked (bottom row). The masked regions were used to calculate the CNR. (c) Violin plot showing a general boost (> 1) in contrast-to-noise ratios after deconvolution..

240 retrievable from text files, and the performance of the overall reconstruction workflow is summarised
 241 in a human-readable, automatically generated report.

242 **4.1. Future work**

243 The case studies in this work have demonstrated that there are differences in the resultant tomograms
 244 from different reconstruction workflows. The reports generated by Ot2Rec also incorporate perfor-
 245 mance statistics from the individual plugins, e.g., shifts between patches in fiducial-less IMOD tilt
 246 series alignment. However, independently measured quality metrics for each stage of the workflow
 247 would enable a more equitable comparison of different software tools, so the user (and eventually
 248 an algorithm) can quantitatively choose the best combination of software tools and the optimum
 249 input parameters for each. The next steps for improving the Ot2Rec reporting system will include
 250 development and implementation of such metrics. For example, Fourier Ring Correlation between
 251 reconstructions of even and odd projections is a commonly adopted, though computationally intensive,
 252 measure of resolution in final tomograms, which could be used to compare reconstruction tools if they
 253 are applied on the same aligned tilt series⁽³⁸⁾. In the future, tomograms could be reconstructed with a
 254 pre-defined range of software tools and selected input parameters, and the best overall workflow could
 255 be determined quantitatively and then applied to other tilt series in the experiment.

256 In the case study from Section 3.3, the difference in motion correction shifts between the first 12
 257 and the remaining tilt series was easily observed from the plot of shifts for all tilt series in the project.
 258 Observing performance of the tomogram reconstruction process over time can be used as an indica-
 259 tion of the quality of the upstream processes (sample preparation, data collection, microscope health)
 260 - enabling facility managers to capture valuable data to correct issues at these stages efficiently. Per-
 261 formance in specific metrics could help troubleshoot potential issues, for example, consistent large
 262 deviations between calculated and input tilt angles from the alignment process could be a sign of issues
 263 with the microscope stage. Issues with poor quality images at specific tilt angles could also be detected
 264 and these images excluded from subsequent analysis.

265 Case Study 2 has demonstrated that custom image processing tools developed within the Ot2Rec
 266 framework can be integrated easily into existing image processing workflows, which is beneficial
 267 to both developers and users. For developers, maintenance and deployment efforts are significantly
 268 reduced as Ot2Rec already provides implementations for file handling of all intermediate steps in the
 269 tomography process. For users, customised image processing tools can be accessed quickly and tested
 270 alongside their existing workflows, all within a familiar framework.

271 Ot2Rec will also be extended to perform other cryo-ET processing tasks, e.g., denoising tomograms,
 272 3D particle picking or sub-tomogram averaging. Some of these tasks will be supported in Ot2Rec by
 273 developing new plugins for existing software tools, or if no suitable tools are available, bespoke plugins
 274 can be developed which would then be available in conjunction with all the standard plugins in Ot2Rec.
 275 More work is needed to adapt the Ot2Rec architecture to handle iterative tasks which combine steps,
 276 e.g., simultaneous CTF correction and reconstruction as implemented in NovaCTF⁽³⁹⁾ by Obr and
 277 colleagues⁽⁴⁰⁾, or iterative alignment and reconstruction⁽⁴¹⁾. And further work is needed to enable a
 278 more automated approach that combines multiple plugins into a workflow that can be launched with a
 279 single command.

280 **4.2. Conclusion**

281 Ot2Rec currently includes the canonical initial steps of tilt series reconstruction, necessary for either
 282 sub-tomogram averaging or segmentation. Alongside of this, it also contains prototype plugins allowing
 283 for deconvolution of tomograms to enhance contrast. Ot2Rec acts both as an open-source wrapper with
 284 a simple unified plugin structure and a developer and user friendly prototyping tool for new plugins.
 285 The reporting functionality provides easy-to-access information, enabling comparisons and optimisa-
 286 tion of parameters and software packages. The further development of this pipeline opens the door to
 287 options such as automated data processing parameter tuning based on the purpose of data collection
 288 or automatic monitoring of upstream steps such as microscope health. Continued open-source cross-
 289 software development of the cryoET pipeline with a focus on ease-of-interaction for both the user and
 290 developer is the future of cryoET data processing.

291

5. Methods

292

5.1. Sample preparation and image acquisition

293

5.1.1. Case Study 1

294 Details of the sample preparation and image acquisition protocols are available in the original
295 publication for the EMPIAR dataset⁽³⁵⁾.

296 For this study, motion correction of the micrographs was performed using MotionCor2, followed by
297 a fiducial-less (patch tracking based) tilt series alignment using IMOD. The patch-tracking algorithm
298 was configured such that there were 24×24 patches, each patch with the dimensions of 210×203
299 pixels, allowing a 15% overlap between patches. The aligned stacks were binned by a factor of 2 before
300 tomogram reconstruction, which was also performed using the batchruntomography tool in the IMOD suite
301 using the default weighted back-projection (WBP) algorithm. The unbinned thickness of the volume
302 was set to 1920 px ($\approx 861\text{\AA}$), such that after the overall factor-2 binning, the dimensions of the output
303 tomograms are $1920 \times 1856 \times 1920$ pixels, with the pixel spacing of 4.486\AA in all dimensions. Specific
304 parameters used in Ot2Rec for this case study are in Table S1.

305 In all case studies presented in this paper, processing was performed on a virtual machine with 12
306 Intel Xeon Gold 5218 2.30GHz CPUs and 1 Tesla V100 GP.

307

5.1.2. Case Study 2

308 JEG-3 human choriocarcinoma cell line was purchased from Merck Life Science (UK) and cultured in
309 Dulbecco's modified Eagle's media (DMEM/F-12, HEPES, Gibco, 11330057) supplemented with 10%
310 fetal bovine serum (Gibco, 10500) and 1% Penicillin-streptomycin (10,000U/ml, Gibco, 11548876).
311 Cells were cultured in T75 flasks and incubated at 37°C with 5% CO_2 .

312 200 mesh gold holey carbon grids (either R2/2 Quantifoil or R3.5/1 Quantifoil, Agar scientific) were
313 sterilised by dipping into 100% ethanol for 2-5min and rinsing with phosphate buffered saline (PBS)
314 (Gibco, 10010). The grids were coated with $30\mu\text{l}$ of 1:20 fibronectin (Merck, F0895) in PBS, and kept
315 in the incubator for 2 hours. The grids were then rinsed with PBS two times and put in a petri dish
316 containing JEG-3 media, and incubated at 37°C and 5% CO_2 for overnight.

317 Prior to cell seeding, the grids were transferred into a 6-well plate (one grid per well) containing
318 fresh JEG-3 media. A total number of trypsinised JEG-3 (3×10^4 cells) were seeded directly onto each
319 grid. The cells were then allowed to settle in the incubator for 2-3 days until they were well spread on
320 the grids.

321 For vitrification, the GP2 (Leica) was used. The humidity-controlled chamber was set to reach $>80\%$
322 humidity. After the grid containing the cells was placed into the GP2, a $2.5 \mu\text{l}$ JEG-3 medium droplet
323 was applied onto the EM grid, and the grid was blotted from the reverse side for 6-10sec. The grid was
324 plunged into liquid ethane, and the frozen grids were stored until focused ion beam (FIB) milling was
325 performed.

326 Prior to the FIB milling, the frozen EM grids were clipped into clip rings (ThermoFisher). Scios
327 scanning electron microscope (ThermoFisher) at the electron Bio-Imaging Centre at Diamond Light
328 Source was used to perform the FIB milling. Gallium ion beams were used to mill the cellular samples
329 to a lamella thickness of 200nm. The ion beam parameters were set to 30kV beam energy, and 50pA -
330 0.3nA beam current (for coarse milling) and 30pA (for fine milling). The grids with FIB-milled lamellae
331 were stored again until cryoET was undertaken using a Titan Krios (ThermoFisher Scientific) at 300kV
332 at eBIC. Each tilt series had 41 projections taken at -53° to $+27^\circ$ degrees in increments of 2° using
333 a dose symmetric imaging scheme⁽¹⁸⁾. Data were collected using a Falcon 4i SelectrisX at $64,000\times$
334 magnification ($1.97 \text{\AA}/\text{pixel}$).

335 Motion correction of the micrographs was first performed with MotionCor2, followed by the esti-
336 mation of the true defocus values using CTFFind4 on a *per-micrograph* basis. The CTFFind4 outputs
337 were then processed using the CTFSim plugin, an Ot2Rec prototype feature, which also simulated and
338 internally reconstructed the 3D PSF of the tilt series. The PSF volumes were truncated to the central
339 $30 \times 30 \times 30$ pixels as the PSF is fast-declining by nature.

340 Fiducial-less tilt series alignment was performed on the motion-corrected micrographs using IMOD.
 341 The patch-tracking algorithm in IMOD was configured such that there were 24×24 patches, each
 342 patch with the dimensions of 224 pixels squared, allowing a 15% overlap between patches. The aligned
 343 stacks were binned by a factor of 8 before tomogram reconstruction. Reconstruction was also performed
 344 using the batchruntom0 tool in the IMOD suite, and the default weighted back-projection (WBP) was
 345 used. The final tomograms have a thickness of 1496Å, which translates to an overall dimensions of
 346 $512 \times 512 \times 1000$ pixels, given an overall binning factor of 8.

347 Lastly, the reconstructed tomograms were deconvolved using the RLDeconv tool in Ot2Rec, with the
 348 corresponding simulated PSF volumes as deconvolution kernels. Specific parameters used in Ot2Rec
 349 for this case study are in Table S2.

350 The contrast-to-noise ratio (CNR), as defined in Eq. (1)⁽³⁶⁾, was used to compare the tomograms
 351 before and after deconvolution with CTFSim and RLDeconv.

$$352 \text{CNR} = \frac{|\mu_1 - \mu_2|}{\sqrt{\sigma_1^2 + \sigma_2^2}} \quad (1)$$

352 where $\mu_1, \mu_2, \sigma_1, \sigma_2$ are the average grey-values of the signal, that of the background, the standard
 353 deviation of signal grey-values, and that of the background grey-values respectively.

354 The CNR was calculated from the central 90% of the original and deconvolved volumes in the
 355 z-direction. Then for each z-slice in a volume, the Ōtsu threshold⁽³⁷⁾ was calculated and used for sep-
 356 arating ¹ the signal from the background (cf. masks shown in red in the second row of Fig 4b). The
 357 CNRs of the i -th z-slices of the two volumes were calculated using Eq. (1). The ratio between the
 358 CNR of the deconvolved volume and that of the original tomogram was calculated to gauge the extent
 359 of enhancement in image contrast. A value over 1 signifies a positive boost in image contrast after
 360 deconvolution.

361 5.1.3. Case Study 3

362 Primary cortical neurons of embryonic C57BL/6J mice were dissociated and seeded on Quantifoil® R
 363 2/2 SiO2 Au200 grids that were glow discharged using a GloCube® Plus (Quorum) at 20mA for 30s
 364 and treated with 0.1mg mL⁻¹ Poly-D-Lysine (Gibco) at 37°C overnight and rinsed with PBS and left to
 365 dry. Cells were seeded onto grids and maintained in Neurobasal® Medium (Gibco) supplemented with
 366 B-27TM (Gibco), 1% penicillin/streptomycin (Gibco), 2mM Glutamate (Gibco). 20% of the volume of
 367 old media was replaced with fresh media every 3-4 days. Cells were plunge frozen on DIV 14.

368 Data were collected with a Titan Krios G4 (ThermoFisher Scientific) transmission cryo-electron
 369 microscope at 300kV equipped with a cold field emission source gun, a Selectris (ThermoFisher Sci-
 370 entific) electron imaging filter, and a post-imaging filter mounted Falcon 4 (ThermoFisher Scientific)
 371 direct electron detector. Tilt series were acquired at 81,000 \times magnification (pixel size 1.47Å) in a dose
 372 symmetric tilt scheme⁽¹⁸⁾ with a tilt range of -60° to 60° imaging at 3° increments, with 2e⁻/Å dose
 373 per tilt image. Tilt series were acquired using Tomography software (ThermoFisher Scientific) and
 374 collected as EER files⁽⁴²⁾.

375 Motion correction was first performed with MotionCor2⁽²⁶⁾. Next, fiducial-less tilt series alignment
 376 was performed with IMOD^(29,30) and AreTomo 1.1.0⁽³¹⁾. In both cases, a binning factor of 8 was
 377 used. The IMOD aligned data was reconstructed with three methods: IMOD simultaneous iterative
 378 reconstruction technique (SIRT), AreTomo simultaneous algebraic reconstruction technique (SART),
 379 and Savu conjugate gradient least squares (CGLS) reconstruction via the ASTRA reconstruction tool-
 380 box⁽⁴³⁻⁴⁵⁾. The AreTomo aligned tilt series was reconstructed with AreTomo SART and Savu CGLS,
 381 though IMOD reconstruction will be supported in later versions of Ot2Rec. Specific parameters used
 382 in Ot2Rec for this case study are in Table S3.

¹NB. This is only a rudimentary measures to pick out potential signals, and is by no means an attempt to automatically segment useful features from the slice.

383 **5.2. Prototype features**

384 *CTFSim*. As mentioned previously, the program CTFFind4 is a tool used for estimating the *true* defocus value for each micrograph collected. However, whilst it produces parameters for determining the 385 shape of the contrast transfer function (CTF) associated with the microscope settings, it does not 386 directly have the CTF as a standard output. In view of this, we developed an in-house plugin, named 387 CTFSim, to simulate the CTF of the micrograph by reverse-engineering the equations described in the 388 Rohou *et al.* paper^(28,46)

$$389 \quad CTF(\lambda, \mathbf{g}, \Delta f, C_s, \Delta\varphi, w_2) = -\sin(\chi(\lambda, \mathbf{g}, \Delta f, C_s, \Delta\varphi, w_2)) \quad (2)$$

390 with

$$\chi(\lambda, \mathbf{g}, \Delta f, C_s, \Delta\varphi, w_2) = \pi\lambda|\mathbf{g}|^2 \left(\Delta f - \frac{1}{2}\lambda^2|\mathbf{g}|^2 C_s \right) + \Delta\varphi + \arctan\left(\frac{w_2}{\sqrt{1-w_2^2}}\right) \quad (3)$$

391 where λ is the associated electron wavelength, \mathbf{g} is the spatial frequency vector, Δf is the defocus value 392 evaluated from CTFFind4, C_s is the spherical aberration, $\Delta\varphi$ is the phase shift, and the value w_2 is 393 associated with the relative phase contrast w_1 via the relation $w_1 = \sqrt{1-w_2^2}$.

394 By definition, the CTF is a function defined in the complex reciprocal space, and is hence rather 395 difficult to visualise and use "as is". Therefore, an additional feature of the CTFSim is to convert the 396 simulated two-dimensional CTF to the point spread function (PSF) in the real space via a direct inverse 397 Fourier transform. Lastly, since the CTF (and PSF) are calculated using the size of the motion-corrected 398 micrographs, these images would have the same size of those micrographs. However, due to the quick- 399 decaying feature of the PSF, the user can choose to truncate the resultant PSF image to a certain size 400 (e.g. 30 pixels squared, by default) in order to facilitate further usage of the obtained results.

401 Once the per-micrograph 2D PSF profiles for a tilt-series are simulated, CTFSim reconstructs the 402 profiles internally using the Weighted Backprojection (WBP) algorithm into a tomogram of the PSF.

403 As suggested in Croxford *et al.*⁽⁴⁷⁾, the *cropped* 3D PSF is post-processed in a three-step process. 404 The PSF tomogram is firstly converted into the 3D CTF with a Fourier transform. Then the pixels are 405 "normalised"² through a division by the value at zero-frequency (i.e. $|\mathbf{g}| = 0$). Lastly, the normalised 406 CTF stack is converted back to the PSF in real-space via an inverse Fourier transform.

407 Finally, the processed PSF is then normalised by dividing the array elements by the global maximum 408 of the array. Although it can be derived trivially from eq. 5 that the analytical output of the iterations 409 should be independent of a linear scaling of the PSF, numerically speaking it is still a multi-step process 410 and an unnormalised PSF could potentially cause numerical instabilities especially in the first fraction 411 in eq. 5. Therefore we assert that if the PSF is to be used to deconvolve the raw tomogram via the 412 Richardson-Lucy scheme, this extra operation is necessary.

413 *RLFDeconv*. The blurring of images due to the optical or electronic properties of the PSF has long been 414 a concern for microscopists. In transmission electron microscopy, the obtained image can be modelled, 415 in the simplest form, as⁽⁴⁸⁾

$$416 \quad I_0 = I_{perf} \otimes PSF + \mathcal{N} \quad (4)$$

417 where I_0 is the final output image, I_{perf} is the perfect image, \mathcal{N} is a stochastic noise term obeying 418 Poisson distribution, and \otimes denotes the convolution operation. In order to reverse-engineer the perfect 419 image I_{perf} , an inverse operation must be carried out. We note that Eq. 4 cannot be solved exactly with 420 any analytical or numerical method, since the noise term is unknown and cannot be isolated from the 421 output image. Hence to obtain a reasonable solution, an approximation is necessary. Here a common

422 ²We acknowledge that this use of "normalisation", directly quoted from the source, may be an abuse of terminology, as the 423 normalisation of a complex matrix is usually defined as the division by the norm of the matrix of associated moduli, rather than 424 by the value at $|\mathbf{g}| = 0$.

418 approximation is that the image signal-to-noise ratio is high enough such that the noise contribution
 419 can be ignored.

420 However, even with such approximation, the inverse of a convolution is still unsolvable by any ana-
 421 lytical means, as the solution is non-unique. Therefore one needs to resort to an iterative approach
 422 numerically. In 1972 and 1974, Richardson and Lucy separately discovered an iterative scheme^(49,50)
 423 that gives an approximation approaching an ideal solution as the number of iteration increases.
 424 Mathematically, the scheme reads

$$I_{i+1} = \left(\frac{I_0}{I_i \otimes PSF} \otimes \overline{PSF} \right) I_i \quad (5)$$

$$\lim_{i \rightarrow \infty} I_i = I_{perf} \quad (6)$$

425 where I_i is the image in the i -th step, and the over-bar on PSF denotes a flip operation of the PSF ,
 426 hence $\overline{PSF(x)} \equiv PSF(-x)$.

427 In Ot2Rec, rather than developing an in-house solver, we have implemented a wrapper plugin for
 428 the Python library RedLionfish⁽⁵¹⁾ for performing the 3-dimensional deconvolution between a recon-
 429 structed tomogram and a simulated PSF stack (similarly reconstructed as the experimental tomogram).
 430 To facilitate the deconvolution of larger stacks, which might cause GPU/CPU memory issues, we also
 431 implemented the 3D version of the so-called "block-iterative" algorithm, inspired by Lee⁽⁵²⁾, which
 432 breaks the volume (tomogram) into chunks, on each of which a normal Richardson-Lucy deconvolu-
 433 tion is performed independently. The separately deconvolved chunks are then stitched back together. A
 434 merit of this method is that due to the massive reduction in the size of deconvolution operands, a much
 435 lower memory cost for the GPU/CPU can be achieved. However, the authors would like to empha-
 436 size that this block-iterative method must be used with care, as the padding setting in the convolution
 437 operations could introduce artefacts around the borders of the chunks as they are stitched back.

438 5.3. Basic usage guide

439 This short section is dedicated to explain the basics of user interaction with Ot2Rec.

440 5.3.1. Installation

441 Ot2Rec is an open-source Linux-based program. Its code repository can be accessed at <https://github.com/rosalindfranklininstitute/Ot2Rec>.

443 The easiest way to install Ot2Rec is to download the shell script of the latest release from the Release
 444 tab on GitHub and execute the script on the command line.

445 An alternative method of installation, should the user wish to build the software from source, is to
 446 clone the repository to the local environment. As Ot2Rec uses miniconda, it is recommended that the
 447 user first create a new conda virtual environment ("venv") with Python 3.8 (or above) pre-installed.
 448 Once the venv is loaded, the user can then use the command `pip install .` in the cloned root
 449 folder to automatically install Ot2Rec and its dependencies locally.

450 5.4. Basic usage

451 Once the virtual environment has been activated, all Ot2Rec command-line functions are available in
 452 the terminal, which generates the corresponding GUI for each plugin. All Ot2Rec commands follow a
 453 specific format which has been summarised in Table 2.

454 To start an image processing pipeline with Ot2Rec, the first command to be used is `o2r.new`. With
 455 this, a GUI will be displayed, allowing the user to enter some essential project-dependent parameters,
 456 with which Ot2Rec will aggregate the master metadata for downstream operations.

457 For subsequent steps, all the plugins contain a `new` and a `run` function. The `new` commands, like the
 458 previous `o2r.new`, prompt the user to input essential parameters for the specified plugin, then collect

Ot2Rec Command	Description
o2r.new	Creates a new Ot2Rec project.
o2r.<plugin>.<function>.new	Creates a new instance of each plugin. For example, o2r.imod.align.new starts a new alignment in IMOD and captures user inputs in the GUI for this plugin. The user parameters are stored in a yaml file.
o2r.<plugin>.<function>.run <proj_name>	Runs the commands that perform the plugin's functions on the project where <proj_name> is the project name. For example, o2r.imod.align.run TS runs IMOD alignment on all tilt series in project TS, which has user parameters stored in TS_align.yaml created from o2r.imod.align.new.
o2r.report.run <proj_name> --to_html --to_slides	Generate the report for the project <proj_name> as a html document and as slides. Note that this requires the o2r_report environment to be activated (detailed instructions available on Github).

Table 2. *Ot2Rec commands and their descriptions.*

459 and pre-propagate the configuration files with metadata from previous steps. The `run` commands look
 460 for the relevant configuration files and previous metadata records, and execute the specified plugin.
 461 For all `run` operations, the project name (as defined by the user at the beginning with the `o2r.new`
 462 command) is required as a command-line argument, as it is used for seeking the correct configuration
 463 files.

464 **Acknowledgements.** We acknowledge Diamond Light Source for access and support of the cryo-EM facilities at the UK's
 465 national Electron Bio-imaging Centre (eBIC), funded by the Wellcome Trust, MRC and BBSRC. We also thank eBIC for ongoing
 466 collaboration and feedback on Ot2Rec and providing the initial scripts on which Ot2Rec was based.

467 We also thank the Core Team at the Artificial Intelligence & Informatics Theme at the Rosalind Franklin Institute, especially
 468 Drs. Joss Whittle and Laura Shemilt, for their help in configuring the computing infrastructure for running and testing of Ot2Rec.

469 **Funding Statement.** The Rosalind Franklin Institute is funded by UK Research and Innovation through the Engineering and
 470 Physical Sciences Research Council. Funding was also provided by the Wellcome Trust through the Electrifying Life Science
 471 grants 220526/Z/20/Z.

472 **Competing Interests.** M.C.D. is an employee of SPT Labtech. The remaining authors declare that they have no competing
 473 interests

474 **Data Availability Statement.** The GitHub repository of Ot2Rec is open-source and can be accessed at <https://github.com/rosalindfranklininstitute/Ot2Rec>. Ot2Rec Report is also open-source and is available at https://github.com/rosalindfranklininstitute/ot2rec_report. All data used in this manuscript can be found on EMPIAR (case study 1: EMPIAR-10364; case study 2: EMPIAR-XXXXXX; case study 3: EMPIAR-XXXXXX).

478 **Ethical Standards.** The research meets all ethical guidelines, including adherence to the legal requirements of the study country.

479 **Author Contributions.** Software development: NBY; EMLH. Data acquisition: WT; JLRS; MG. Data processing: NBY;
 480 EMLH. Writing original draft: NBY; EMLH; WT; MD; MCD; MB. All authors approved the final submitted draft.

481 **Supplementary Material.**

- 482 • Ot2Rec Report for Case Study 1
- 483 • Ot2Rec Report for Case Study 2
- 484 • Ot2Rec Report for Case Study 3 - IMOD
- 485 • Ot2Rec Report for Case Study 3 - AreTomo
- 486 • Table S1: Configuration parameters for Case Study 1
- 487 • Table S2: Configuration parameters for Case Study 2
- 488 • Table S3: Configuration parameters for Case Study 3
- 489 • Guide on writing plugins for Ot2Rec
- 490 • Tutorial to reproduce Case Study 1 in Ot2Rec
- 491 • Movie S1: Video of 3D reconstructions from the various workflows in Case Study 3

492 **References**

- 493 1. Schmid M (2011) Chapter 2 - Single-particle electron cryotomography *Adv Protein Chem Struct Biol* **82**, 37–65.
- 494 2. Briggs JAG (2013) Structural biology *in situ* – the potential of subtomogram averaging *Curr. Opin. Struct. Biol.* **23**(2), 261–267.
- 495 3. Förster F & Hegerl R (2007) Structure Determination *In Situ* by Averaging of Tomograms *Methods Cell Biol.* **79**, 741–767.
- 496 4. Schur FKM et al. (2013) Determination of protein structure at 8.5 Å resolution using cryo-electron tomography and 497 sub-tomogram averaging *J. Struct. Bio.* **184**(3), 394–400.
- 498 5. Dai W et al. (2013) Visualizing virus assembly intermediates inside marine cyanobacteria *Nature* **502**, 707–710.
- 499 6. Sutton G et al. (2020) Assembly intermediates of orthoreovirus captured in the cell *Nat. Commun.* **11**, 4445.
- 500 7. Wu GH et al. (2020) Multi-scale 3D Cryo-Correlative Microscopy for Vitrified Cells *Structure* **28**(11), 1231–1237.
- 501 8. Schertel A et al. (2013) Cryo FIB-SEM: Volume imaging of cellular ultrastructure in native frozen specimens *J. Struct. 502 Bio.* **184**(2), 355–360.
- 503 9. Zhu Y et al. (2021) Serial cryoFIB/SEM Reveals Cytoarchitectural Disruptions in Leigh Syndrome Patient Cells *Structure* 504 **29**(1), 82–87.
- 505 10. Dubochet J et al. (1988) Cryo-electron microscopy of vitrified specimens. *Quart. Rev. Biophys.* **21**(2), 192–228.
- 506 11. Dahl R & Staehelin A (1989) High-pressure Freezing for the preservation of biological structure: Theory and practice *J. 507 Electron Microsc. Tech.* **13**(3), 165–174.
- 508 12. Al-Amoudi A et al. (2004) Cryo-electron microscopy of vitreous sections of native biological cells and tissues *J. Struct. 509 Bio.* **148**(1), 131–135.
- 510 13. Krueger R (1999) Dual-column (FIB-SEM) wafer applications *Micron* **30**(3), 221–226.
- 511 14. Hayles MF et al. (2010) The making of frozen-hydrated, vitreous lamellas from cells for cryo-electron microscopy *J. 512 Struct. Bio.* **172**(2), 180–190.
- 513 15. Wolff G et al. (2019) Mind the gap: Micro-expansion joints drastically decrease the bending of FIB-milled cryo-lamellae. 514 *J. Struct. Bio.* **208**(3), 107389.
- 515 16. Peddie C & Collinson LM (2014) Exploring the third dimension: Volume electron microscopy comes of age *Micron* **61**, 516 9–19.
- 517 17. Peddie C et al. (2022) Volume electron microscopy *Nat Rev Methods Primers* **2**, 51.
- 518 18. Hagen W et al. (2017) Implementation of a cryo-electron tomography tilt-scheme optimized for high resolution 519 subtomogram averaging *J. Struct. Bio.* **197**(2), 191–198.
- 520 19. Koning RI et al. (2018) Advances in cryo-electron tomography for biology and medicine *Ann Anat* **217**, 82–96.
- 521 20. Pyle E & Zanetti G (2021) Current data processing strategies for cryo-electron tomography and subtomogram averaging 522 *Biochemical Journal* **478**(10), 1827–1845.
- 523 21. Balschew N & Kudryashev M et al. (2022) TomoBEAR <https://github.com/KudryashevLab/TomoBEAR>.
- 524 22. Pyle E & Zanetti G (2022) Automated Workflow to Pre-Process Raw Tomography Data for RELION 4.0 https://github.com/EuanPyle/reliion4_tomo_robot.
- 525 23. Tang G & Peng L et al. (2007) EMAN2: an extensible image processing suite for electron microscopy *J. Struct. Bio.* **157**, 526 38–46.
- 527 24. de la Rosa-Trevín JM & Quintana A et al. (2016) Scipion: A software framework toward integration, reproducibility and 528 validation in 3D electron microscopy *J. Struct. Bio.* **195**(1), 93–99.
- 529 25. Tegunov D & Cramer P (2019) Real-time cryo-electron microscopy data preprocessing with Warp *Nat Methods* **16**, 1146– 530 1152.
- 531 26. Zheng S et al. (2017) MotionCor2: anisotropic correction of beam-induced motion for improved cryo-electron microscopy. 532 *Nat. Methods* **14**, 331–332.
- 533 27. Mindell JA & Grigorieff N (2003) Accurate determination of local defocus and specimen tilt in electron microscopy. *J. 534 Struct. Bio.* **142**(3), 334–347.
- 535 28. Rohou A & Grigorieff N (2015) CTFFIND4: Fast and accurate defocus estimation from electron micrographs. *J. Struct. 536 Bio.* **192**(2), 216–221.
- 537 29. Kremer J et al. (1996) Computer visualization of three-dimensional image data using IMOD. *J. Struct. Bio.* **116**(1), 71–76.
- 538 30. Mastronarde DN & Held SR (2017) Automated tilt series alignment and tomographic reconstruction in IMOD. *J. Struct. 539 Bio.* **197**(2), 102–113.
- 540 31. Zheng S et al. (2022) AreTomo: An integrated software package for automated marker-free, motion-corrected cryo-electron 541 tomographic alignment and reconstruction. *J. Struct. Bio.* **X** **6**, 100068.
- 542 32. Wadeson N & Basham M (2016) Savu: A Python-based, MPI Framework for Simultaneous Processing of Multiple, N- 543 dimensional, Large Tomography Datasets. *ArXiv: 1610.08015v1*.
- 544 33. Lambert T et al. (2022) napari/magicgui. *Zenodo* <https://doi.org/10.5281/zenodo.7254817>
- 545 34. Kluyver T et al. (2016) Jupyter Notebooks – a publishing format for reproducible computational workflows. *Positioning 546 and Power in Academic Publishing: Players, Agents and Agendas*, 87–90.
- 547 35. Burt A et al. (2020) Complete structure of the chemosensory array core signalling unit in an *E. coli* minicell strain *Nat. 548 Comms.* **11**, 743.
- 549 550

551 36. Timischi F (2015) The contrast-to-noise ratio for image quality evaluation in scanning electron microscopy *Scanning* **37**(1),
552 54–62.

553 37. Ōtsu N (1979) A threshold selection method from gray-level histograms *IEEE Trans. Sys. Man. Cyber.* **9**(1), 62–66.

554 38. Cardone G & Grünwald K *et al.* (2005) A resolution criterion for electron tomography based on cross-validation *J. Struct.*
555 *Bio.* **151**(2), 117–129.

556 39. Turoňová B *et al.* (2017) Efficient 3D-CTF correction for cryo-electron tomography using NovaCTF improves subtomogram
557 averaging resolution to 3.4 Å. *J. Struct. Bio.* **199**(3), 187–195.

558 40. Obr M *et al.* (2022) Exploring high-resolution cryo-ET and subtomogram averaging capabilities of contemporary DEDs *J.*
559 *Struct. Bio.* **214**(2), 107852.

560 41. Gürsoy D *et al.* (2017) Rapid alignment of nanotomography data using joint iterative reconstruction and reprojection *Sci.*
561 *Rep.* **7**, 11818.

562 42. Guo H *et al.* (2020) Electron-event representation data enable efficient cryoEM file storage with full preservation of spatial
563 and temporal resolution *IUCrJ* **7**(5), 860–869.

564 43. van Aarle W *et al.* (2016) Fast and flexible X-ray tomography using the ASTRA toolbox *Optics express* **24**(22), 25129–
565 25147.

566 44. van Aarle W *et al.* (2015) The ASTRA Toolbox: A platform for advanced algorithm development in electron tomography
567 *Ultramicroscopy* **157**, 35–47.

568 45. Palenstijn WJ *et al.* (2011) Performance improvements for iterative electron tomography reconstruction using graphics
569 processing units (GPUs) *J. Struct. Bio.* **176**(2), 250–253.

570 46. Fernando KV & Fuller SD (2007) Determination of astigmatism in TEM images. *J. Struct. Bio.* **157**, 189–200.

571 47. Croxford M *et al.* (2021) Entropy-regularized deconvolution of cellular cryotransmission electron tomograms *PNAS*
572 **118**(50), e2108738118.

573 48. Reimer L & Kohl H. (2007) Transmission Electron Microscopy: Physics of Image Formation *Springer 5e.*, .

574 49. Richardson WH (1972) Bayesian-Based Iterative Method of Image Restoration. *JOSA* **62**(1), 55–59.

575 50. Lucy LB (1974) An iterative technique for the rectification of observed distributions. *Astronomical Journal* **79**(6), 745–754.

576 51. Perdigão LMA *et al.* (2022) rosalindfranklininstitute/RedLionfish. *Github* <https://github.com/rosalindfranklininstitute/RedLionfish>

577 52. Lee NY (2015) Block-iterative Richardson-Lucy methods for image deblurring. *EURASIP Journal on Image and Video*
578 *Processing* **2015**, 14.

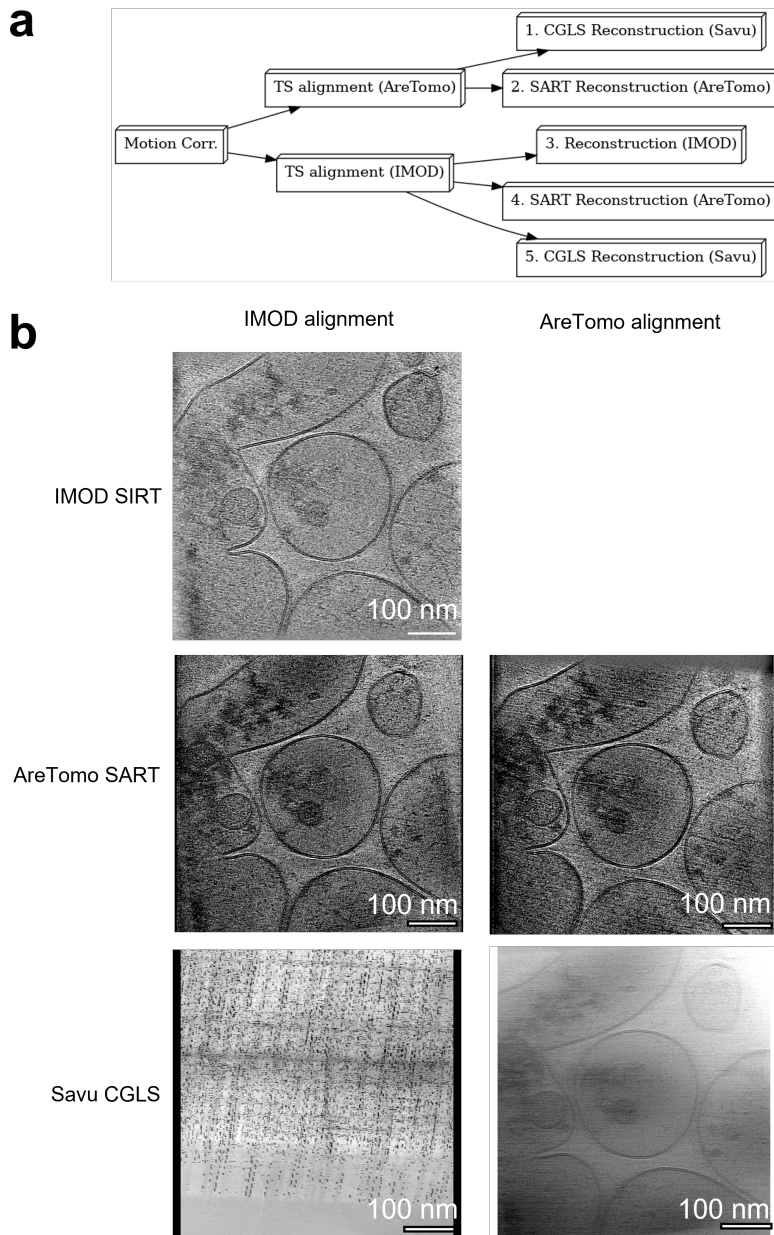


Figure 5. Different combinations of IMOD, AreTomo, and Savu for alignment and reconstruction yielded varying results. Five combinations (1 - 5) were tested, as shown in the workflow diagram a. NB. Iterative reconstruction with CGLS in Savu (Route 5) failed due to poor alignment results from IMOD alignment. However, the same reconstruction method produced a good quality reconstruction when the AreTomo alignment method was used instead (Route 1) (a) Workflow diagram used in Case Study 3, (b) Central x-y slice of the tomogram reconstructed with IMOD, AreTomo, and Savu on IMOD and AreTomo aligned data. Note that IMOD reconstruction with AreTomo aligned data is not available on the current version of *Ot2Rec*, but will be supported in later versions. A movie showing this figure in 3D is available in the Supplementary Information (Movie S1).

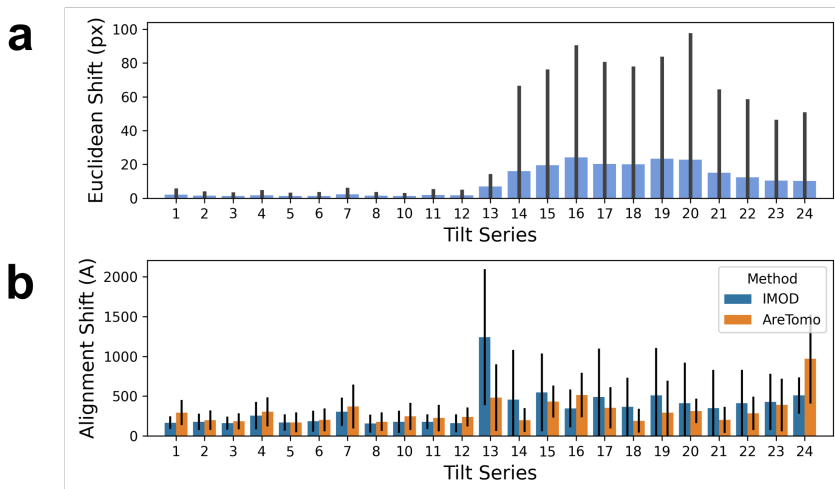


Figure 6. Evaluation of all tilt series shifts from motion correction and alignment at once show substantially larger shifts from tilt series 13 onwards. (a) Euclidean shifts reported by motioncor2 for all tilt series in Case Study 3 (Sect. 3.3) show a large increase from tilt series 13 onwards. (b) Alignment shifts reported by IMOD and AreTomo alignment processes. The alignment shift here is the Euclidean distance between patches which are recorded as metadata from IMOD and AreTomo directly. In both (a) and (b), The bar plots represent the mean and the error bars are the standard deviations in shifts..